Journal of Colloid and Interface Science 512 (2018) 609–617

Contents lists available at ScienceDirect

Journal of Colloid and Interface Science

journal homepage: www.elsevier.com/locate/jcis

Regular Article

Unveiling the hybrid interface in polymer nanocomposites enclosing silsesquioxanes with tunable molecular structure: Spectroscopic, thermal and mechanical properties

Massimiliano D'Arienzo [a,*], Sandra Diré [b,c,*], Matteo Redaelli [a], Evgeny Borovin [b], Emanuela Callone [b,c], Barbara Di Credico [a], Franca Morazzoni [a], Alessandro Pegoretti [b], Roberto Scotti [a]

[a] Dept. of Materials Science, INSTM, University of Milano-Bicocca, Via R. Cozzi 55, 20125 Milano, Italy
[b] Dept. Industrial Engineering, University of Trento, via Sommarive 9, 38123 Trento, Italy
[c] "Klaus Müller" Magnetic Resonance Lab., DII, University of Trento, via Sommarive 9, 38123 Trento, Italy

GRAPHICAL ABSTRACT

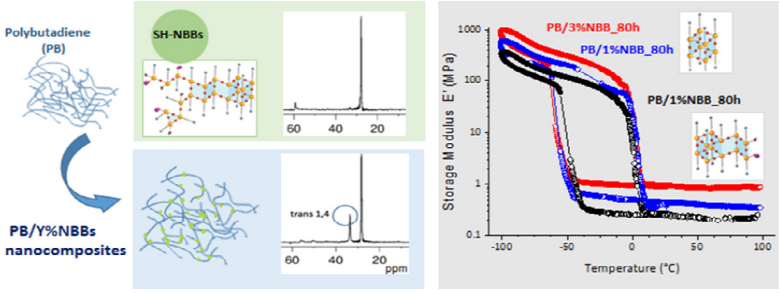

ARTICLE INFO

Article history:
Received 1 August 2017
Revised 20 October 2017
Accepted 24 October 2017
Available online 26 October 2017

Keywords:
Nanocomposite
Silsesquioxanes
Hybrid materials
Interfaces
Nanobuilding blocks
Mechanical properties

ABSTRACT

Organic–inorganic nanobuilding blocks (NBBs) based on silsesquioxanes (SSQs) have potential applications as nanofillers, thermal stabilizers, and rheological modifiers, which can improve thermomechanical properties of polymer hosts. The possibility to tune both siloxane structure and pendant groups can promote compatibilization and peculiar interactions with a plethora of polymers. However, the control on SSQs molecular architecture and functionalities is usually delicate and requires careful synthetic details. Moreover, investigating the influence of NBBs loading and structure on the hybrid interface and, in turn, on the polymer chains mobility and mechanical properties, may be challenging, especially for low-loaded materials.

Herein, we describe the preparation and characterization of polybutadiene (PB) nanocomposites using as innovative fillers thiol-functionalized SSQs nanobuilding blocks (SH-NBBs), with both tailorable functionality and structure. Swelling experiments and, more clearly, solid-state NMR, enlightened a remarkable effect of SH-NBBs on the molecular structure and mobility of the polymeric chains, envisaging the occurrence of chemical interactions at the hybrid interface. Finally, thermal and DMTA analyses revealed that nanocomposites, even containing very low filler loadings (i.e. 1, 3 wt%), exhibited enhanced thermomechanical properties, which seem to be connected not only to the loading, but also to the peculiar cage or ladder-like architecture of SH-NBBs.

* Corresponding authors at: Dept. Industrial Engineering, University of Trento, via Sommarive 9, 38123 Trento, Italy (S. Diré).
E-mail addresses: massimiliano.darienzo@unimib.it (M. D'Arienzo), sandra.dire@unitn.it (S. Diré).

https://doi.org/10.1016/j.jcis.2017.10.094
0021-9797/

1. Introduction

Silsesquioxanes (SSQs) represent a unique family of organic–inorganic hybrid materials, which exhibit or impart, if included in polymer composites, a number of beneficial properties, e.g. excellent thermal stability, low dielectric constant, good mechanical properties, chemical resistance, and even biocompatibility [1–8]. SSQs can assume various structural forms and serve different applications, due to the marriage of the siloxane bond networks with organic constituents [1–10]. Three main classes are generally reported: random branched polymers, polyhedral oligomeric silsesquioxanes (POSS), and ladder-like polysilsesquioxanes (LPSQs). Among them, only POSS and LPSQs possess a tailorable and controlled structure, and effectively provide significant mechanical properties. In detail, POSS generally present oligomeric three-dimensional cage structure formed by an inorganic silica-like core (Si_8O_{12}) surrounded by eight covalently bonded organic (polar or nonpolar) groups (R_8), while a typical LPSQ is a polymeric analogue with a linear, double-strained siloxane backbone provided by organic functionalities [1–10].

SSQs were successfully incorporated in various polymers such as polyolefins, polyesters, polyamides, styrenics, acrylates, polyurethanes and thermosettings [1,11–13]. For instance Matejka et al. [14] prepared rubbery epoxy-POSS hybrid composites by incorporating a novel diepoxy-POSS monomer in an epoxy network and then initiating the polymerization. They suggested that not only the amount of the nanofiller, but also the organization of the POSS nanounits determine the nanocomposites performances. In detail, POSS units self-assemble to form crystalline lamellae in the epoxy matrix, which serve as network physical junctions and severely restrict the polymer chains mobility, inducing a pronounced reinforcement to the neat polymer.

Similar investigations have been performed for LPSQs [15–18]. Recently Cho et al. [19], prepared a highly compatible inorganic-organic hybrid Polyvinylidene fluoride (PVDF)/UV-Curable LPSQ composites. The LPSQ contained both phenyl and methacryl groups which promoted hydrogen-bonding with the PVDF backbone and enhanced mechanical robustness after UV-curing.

Many other studies demonstrated the improved properties of polymer-SSQs hybrid nanocomposites, whose extent remarkably depends on the filler amount, dispersion, structure (ladder, cage) and chemical nature of the pendant groups [20–25]. Nevertheless, investigating the influence of SSQs on the hybrid interface and, in turn, on the polymer chains mobility and mechanical properties may be a challenging task, especially for low-loaded materials.

Thus, it appears highly innovative exploring the possibility to produce polymer nanocomposites enclosing SSQs bearing specific and fixed functional groups, and with tunable cage/ladder-like molecular structure.

However, the control on the final molecular architecture and functionalities of such systems is usually a delicate process, which requires a careful tailoring and understanding of synthetic details, in order to avoid possible side reactions (cross-linking, cyclization and gelation). In this context, Dirè et al. [26,27] have recently reported a relatively simple protocol for obtaining thiol-functionalized SSQs nano-building blocks (SH-NBBs; average hydrodynamic diameter ~2 nm) with tunable cage-like or ladder-like structure (Fig. S1, Supplementary Information), by using an *in-situ* water production (ISWP) sol-gel strategy. These species may represent therefore suitable candidates for the preparation of nanocomposites with defined properties.

With this aim, low concentrations of SH-NBBs with different molecular structure have been incorporated in *cis* 1,4 polybutadiene (PB), by a simple and rapid *solution-blending* technique.

The thermal properties of the obtained hybrid nanocomposites have been evaluated by differential scanning calorimetry (DSC) and thermogravimetric analysis (TGA). Comprehensive investigation on the interactions between SH-NBBs units and polymer host has been performed by solid-state nuclear magnetic resonance (NMR) spectroscopy, focusing on the effects of SH-NBBs incorporation on the molecular structure and mobility of the polymeric chains. Further, the mechanical properties of the novel nanocomposites have been explored through dynamic mechanical thermal analysis (DMTA) measurements.

It turned out that even very low SH-NBBs loadings (i.e. 1 and 3 wt%) induce both a significant reduction of polymer chains mobility and a remarkable enhancement of the mechanical performances, also depending on the molecular architecture of the filler.

The overall outcomes demonstrate that these peculiar SSQs are readily applicable in functional nanocomposites with tailorable properties and indicate the efficacy of the methodological approach adopted in providing insights into the hybrid interface between small molecular nanobuilding blocks and polymer hosts.

2. Experimental

2.1. Materials

(3-Mercaptopropyl)trimethoxysilane (McPTMS) and dibutyltindilaurate (DBTL) were purchased from ABCR GmbH (Germany) and used without any further purification. Chloroacetic acid (ClAA) and 1-propanol (1-PrOH), Polybutadiene, cis (average M_w 200,000–300,000) and toluene were purchased from Sigma–Aldrich and used as received.

2.2. Synthesis of SH-NBBs

The preparation of SH-NBBs was performed according to the procedure already reported [27]. In detail, SH-NBBs were synthesized from McPTMS by using the in-situ water production (ISWP) process in which the water needed to hydrolyze the precursor was provided by an esterification reaction between 1-PrOH and ClAA. The water provided through the esterification reaction of ClAA and 1-PrOH enabled the hydrolysis-condensation of McPTMS. The synthesis was carried out under a nitrogen atmosphere using Schlenk technique, the solvents were dried before use by following standard procedures, and the glassware used for reactions was dried in oven at 80 °C for 24 h prior to use. McPTMS (465 μL, 2.5 mmol) was diluted in PrOH (3.36 mL) in a self-condensing Schlenk flask. ClAA (1.417 g) and the condensation promoter DBTL (22 μL) were then added to the solution under vigorous stirring. The clear solution was left reacting at 100 °C for 30 h and 80 h respectively, keeping its initial transparency and homogeneity. No precipitate was ever observed after the analyzed reaction times. The assessed yield in cage-like and ladder-like structures was demonstrated to depend on the reaction time according to Attenuated Total Reflection–Fourier Transform InfraredSpectroscopy (ATR–FTIR), Gel permeation chromatography (GPC) and NMR results. After 30 h reaction SH-NBBs were characterized mainly by ladder-like structures whereas the maximum amount of cage-like structures was obtained after 80 h.

Hereafter the different thiol-functionalized NBBs will be labeled as SH-NBB_Xh where Xh refers to the different reaction times in hours (Xh = 30 h or 80 h).

2.3. Preparation of nanocomposites

SH-NBBs synthesized at different reaction times (30 and 80 h) have been incorporated in PB to produce nanocomposites, according to the procedure shown in Scheme 1.

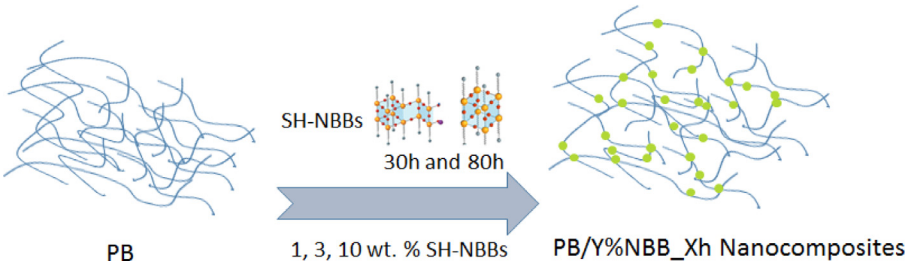

Scheme 1. Experimental procedure for the preparation of PB/Y%NBBs nanocomposites.

Pre-dried PB was dissolved overnight in toluene. The resulting solution was split into different flasks for the addition of different amounts of SH-NBBs solutions. In a typical procedure, PB (2 g) was dissolved in 40 mL of anhydrous toluene. Then, different loadings of SH-NBBs (1, 3, 10 wt%) were added to the polymer solution and stirred for 2 h under N_2 flow. The obtained solutions were cast in Petri dishes and the volatiles were removed overnight by maintaining the system under an aspiration hood. Finally, the complete elimination of the by-products from the composites was achieved by heating the samples at 70 °C for 1 h under vacuum. At a visual inspection, all obtained samples were homogeneous and transparent.

Hereafter the different nanocomposites will be labeled PB/Y% NBB_Xh where Y refers to the different percentage of SH-NBBs (Y = 1, 3, 10 wt%), while X denotes the different reaction times (Xh = 30 or 80 h).

2.4. Characterizations of PB/Y%NBB_Xh nanocomposites

In order to verify the effective presence of SH-NBBs in the polymer matrix, ATR–FTIR measurements were performed on a Perkin Elmer Spectrum 100instrument (1 cm^{-1} resolution spectra, 650–4000 cm^{-1} region, 16 scans).

Solid state NMR analyses were carried out with a Bruker 300WB spectrometer operating at a proton frequency of 300.13 MHz, with the aim of elucidate the structure and the NBBs-polymer interactions in the nanocomposites. The NMR experiments were run on PB/Y%NBB_Xh nanocomposites, and on a sample prepared *ad-hoc* for the NMR analysis with incorporation of 30 wt% of SH-NBBs_80h, namely PB/30%NBB_80h. Magic angle Spinning (MAS) NMR spectra were acquired with proton decoupled single pulse and cross polarization pulse sequences under the following conditions: ^{13}C frequency: 75.47 MHz, $\pi/2$ pulse 3.5 μs, decoupling length 5.9 μs, recycle delay: 30 s, 1 k scans; variable contact time (VCT) experiments: range 200–9000 μs, recycle delay 5 s. Samples were packed in 4 mm zirconia rotors, which were spun at 7 kHz under air flow. Adamantane was used as external secondary reference. Bruker TopSpin software was used for the lineshape analysis. The results were considered acceptable with confidence level of 95%.

TGA was performed in order to study the thermal properties between NBBs and polymer. TGA thermograms were collected by using a Mettler Toledo TGA/DSC1 STARe system at constant gas flow (50 cm^3 min^{-1}). The sample powders were heated in air from 30 to 1000 °C at a heating rate of 10 °C min^{-1}. TGA curves were used to determine the temperature-dependent mass loss of SH-NBBs, giving an indication of the relation between structure and thermal properties.

Differential Scanning Calorimetry (DSC) tests were performed through a DSC30 module by Mettler-Toledo (Columbus, OH, USA). Aluminum pans were used and the sample weight was approximately 15–20 mg. Tests were performed under a nitrogen flow of 100 ml/min. All samples were first heated from −130 to 100 °C then cooled from 100 to −130 °C and a second heating scan up to 100 °C is finally performed. Heating and cooling steps were carried out with the same rate of 10 °C/min. The glass transition temperature (T_g) was determined as the inflection point of the thermograms, while melting (T_m) and crystallization (T_c) temperatures were determined at the maximum endothermic and exothermic peaks, respectively. The enthalpy of fusion (H_m) and crystallization (H_c) were calculated from the endothermic and exothermic peaks.

Swelling and extraction experiments were performed on PB%/NBB nanocomposites to evaluate the cross-linking density.

Samples of 10 × 10 × 2 mm^3 (0.20 ± 0.02 g) were immersed in close vessels filled with 10 mL of toluene at 25 °C for three days in the dark, to avoid photodegradation reactions. Toluene swells the composites and extracts the polymer chains not bound to silica or not crosslinked. It was replaced daily by fresh solvent to eliminate all the extractable chains. Finally, the swollen mass was weighted and dried till constant mass under vacuum at 70 °C for 12 h. Under the same conditions, uncured neat PB completely solved in toluene.

In order to evaluate the cross-linking density of the nanocomposites, the volumetric fraction of the swelled rubber V_r was calculated according to the following equation [28]:

$$V_r = \frac{(m_d - fm_0)\cdot \rho_p^{-1}}{(m_d - fm_0)\cdot \rho_p^{-1} + m_{so}\cdot \rho_s^{-1}} \quad (1)$$

where: $m_{so} = (m_{sw} - m_d)$ is the weight of the solvent in the swollen mass; m_{sw} is the weight of the swollen mass; ρ_p = 0.94 g cm^{-3} is the PB density; ρ_s = 0.87 g cm^{-3} is the toluene density; f is the fraction of the filler in the composites as determined by TGA. The cross-link density v, i.e. the number of network chains per gram bounded on both ends by crosslinks, was calculated according the Flory-Rehner equation [29]:

$$v = \frac{[\ln(1 - V_r) + V_r + \chi V_r^2]}{-2\cdot \rho_p \cdot V_s \cdot (V_r)^{1/3}} \quad (2)$$

where V_s = 105.91 cm^3 mol^{-1} is the molar volume of toluene and χ is the Flory solvent-polymer interaction term, which is 0.472 for toluene-PB [30].

The experimental uncertainty on the reported v values does not exceed ±10%.

DMTA measurements were carried out by a DMA Q800 apparatus from TA Instruments (New Castle, DE, USA) in tensile mode. A rectangular specimen (gauge length of 12 mm; pre-stress of 0.01 N; sinusoidal strain with a frequency of 1 Hz and amplitude of 0.05%) was first cooled from room temperature to −100 °C at a heating rate of 5 °C/min and then heated from −100 up to 100 °C at a heating rate of 3 °C/min. Storage modulus and loss modulus were measured and compared as a function of temperature.

3. Results

3.1. Characterizations of PB/Y%NBB_Xh nanocomposites

Although already reported in previous studies, [26,27] the FTIR characterization of SH-NBB_30 h and SH-NBB_80 h has been repeated (Fig. S2) in order to better discuss the effect of their incorporation in the PB matrix.

Both SH-NBBs samples show a very broad and intense absorption between 3750 and 3000 cm^{-1} attributable to the stretching of OH groups deriving from 1-PrOH utilized as reaction solvent, and a band at 1760 cm^{-1} due to the C=O stretching vibration of both residual ClAA and esterification products (Fig. S2a).

The Si–O asymmetric stretching vibrations are detectable in the 1200–900 cm^{-1} range; the magnification of this spectral region is reported in Fig. S2b where the vibrations attributed to cage-like and ladder-like species are also highlighted. Even though the presence of intense bands due to 1-PrOH makes complicate a careful spectra analysis, the slight increase in intensity of the T^8 cage band centered at 1135 cm^{-1} in the SH-NBBs_80h in comparison with SH-NBBs_30h confirms the preferential formation of cage-like structures at higher reaction time, in accordance to previous comprehensive NMR investigations [27].

The effective incorporation of SH-NBBs in the polymer matrix was preliminary checked by FT-IR spectroscopy (Fig. 1). In detail, Fig. 1a shows the spectra of PB before and after the incorporation of 1, 3, and 10% SH-NBB_80h. As the filler amount increases in the nanocomposites, the typical bands associated to SH-NBBs units become more evident, particularly in the region between 1200 and 900 cm^{-1}. Moreover, an in depth inspection of the spectra reveals that the C=O vibration related to the by-products present in SH-NBBs increases (Fig. 1b). Similar results have been achieved for PB/Y%NBB_30h nanocomposites (spectra not shown).

In order to preliminary explore the possible influence of SH-NBB molecular architecture on the composites properties, a comparison among the FT-IR spectra of PB and nanocomposites loaded with 3 wt% of SH-NBBs synthetized with different reaction times (30 h and 80 h) has been performed (Fig. 1c and d). Differences between the samples can be noticed only in the siloxane region (1250–1050 cm^{-1}).

The SH-NBBs architecture appears substantially unaffected by the incorporation into polymer matrix. As a matter of fact, the

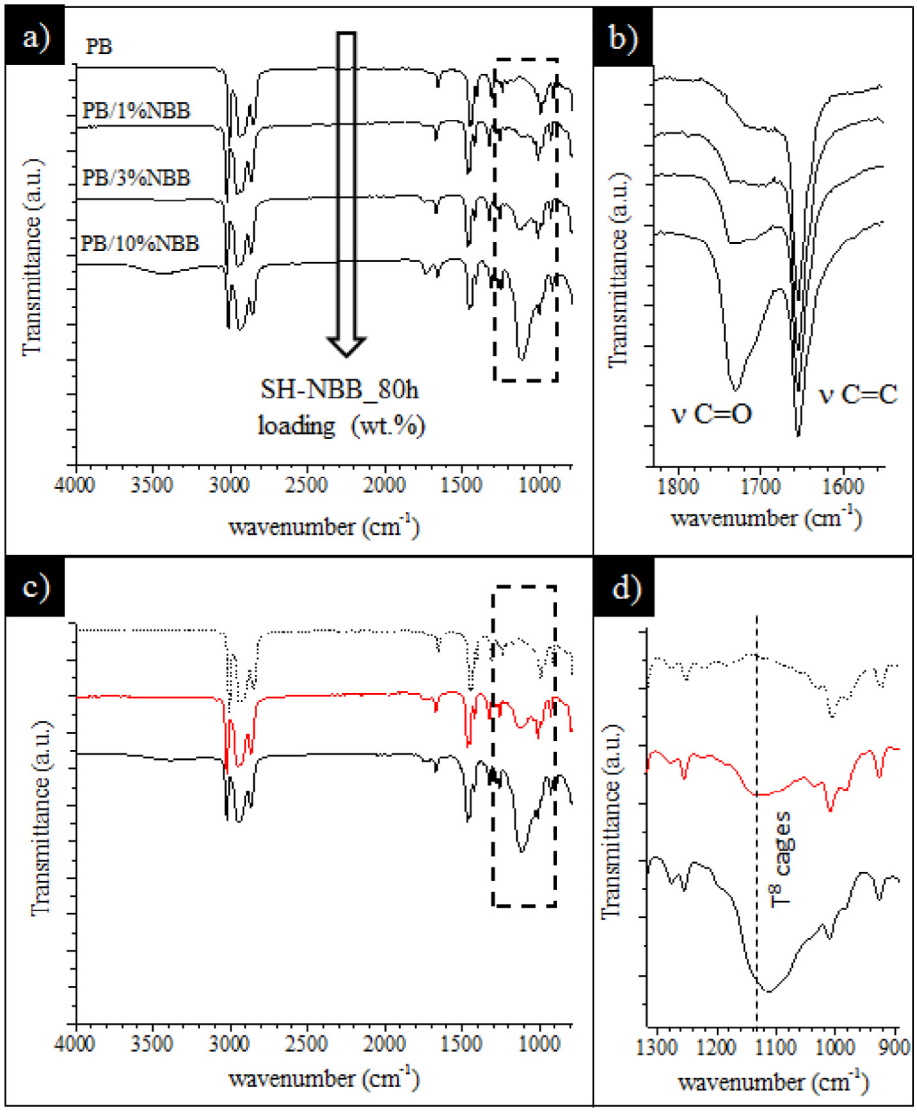

Fig. 1. (a) FT-IR spectra of pure PB and PB/Y%NBB_80h nanocomposites; (b) magnification of the C=O stretching spectral region; (c) FT-IR spectra of pure PB (black dotted line), PB/3%NBB_80h (red line) and PB/3%NBB_30h (black line); (d) magnification of the siloxane spectral region. (For interpretation of the references to colour in this figure legend, the reader is referred to the web version of this article.)

ν_{as}(Si-O) band of PB/3%NBB_80h shows the presence of cages according to the intensity of the signal at 1135 cm^{-1}. On the contrary, the siloxane band of PB/3%NBB_30h is dominated by signals related to ladder-like species; it is worth of noting that it appears much more intense than in PB/3%NBB_80h (Fig. 1d). These results, beyond indicating the effective incorporation of the SH-NBBs within the polymer matrix, suggest different SH-NBBs behavior in the composites as a function of their structure. However, further investigation on the properties of the composites are mandatory to support this hypothesis (see NMR investigation), and in particular to evaluate the role of the SH-NBBs loading and structure in upgrading their mechanical properties.

Swelling experiments were performed on PB/Y%NBB_Xh nanocomposites, in order to evaluate the cross-linking induced by the introduction of SH-NBBs nanounits. In detail, cross-linking density (ν) values were determined according to the Flory-Rehner equation [28,29] (Experimental, Eq. (2)) and the results are summarized in Fig. 2.

For both PB/Y%NBB_30h and PB/Y%NBB_80h nanocomposites the ν values generally increase with the SH-NBBs amount and are very similar at the lowest filler loadings (i.e. for 0.5 and 1 wt %), Interestingly, the reticulation degree becomes remarkably different for PB/3%NBB_30h and PB/3%NBB_80h nanocomposites. In fact, the crosslink density is significantly higher and reaches a maximum for the sample enclosing 3 wt% of SH-NBB_80h units, which possess a larger fraction of cages in their molecular structure (see inset in Fig. 2). These results suggest an effect of the SH-NBBs architecture on the filler-polymer interactions. In particular, they seem to indicate that nanocages in SH-NBBs_80h, thanks to their high number of tunable functionalities concentrated on the same small unit, may provide improved chemical or physical interactions at the polymer-NBBs interface. Therefore, the enhancement of the nanocomposite performance could be expected for PB/3% NBB_80h.

However, at higher loading both PB/10%NBB_30h and PB/10% NBB_80h nanocomposites show a partial depletion of the cross-linking density values. This may be correlated to aggregation phenomena among SH-NBBs, which generally takes place when the filler volume fraction in a nanocomposite becomes relatively high, and appear more pronounced in the case of composites filled with SH-NBBs_80h, containing a larger fraction of cage units.

To further elucidate the structural effects of SH-NBBs incorporation in PB, solid state NMR experiments were performed. The ^{13}C

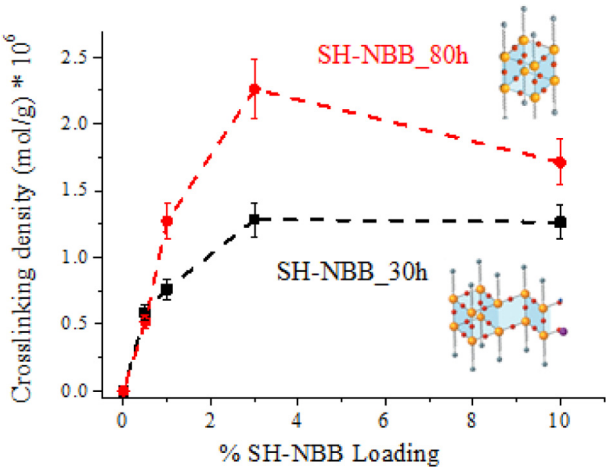

Fig. 2. (a) Trend of the cross-linking density as a function of SH-NBBs loadings for PB/Y%NBB_30h (black line) and PB/Y%NBB_80h (red line). Insets show the molecular architecture corresponding to SH-NBB_30h (bottom) and SH-NBB_80h (top), respectively. (For interpretation of the references to colour in this figure legend, the reader is referred to the web version of this article.)

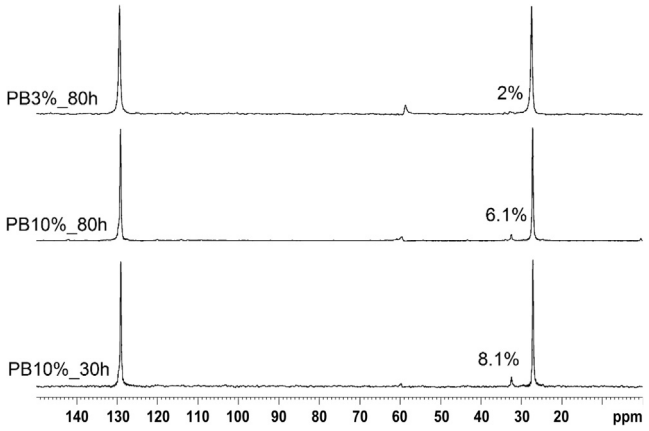

Fig. 3. ^{13}C proton decoupled MAS NMR spectra of PB/3%NBB_80h, PB/10%NBB_80h and PB10%NBB_30h. Peaks at 60 ppm are spinning sidebands.

MAS NMR spectrum of PB (Fig. S3a) shows that the commercial PB polymer is characterized by two main signals at 129.5 and 27.6 ppm, respectively assigned to =CH and —CH_2— functional groups in a cis-1,4 configuration (***c***). The resonances appear quite narrow, because the elastomer functional groups undergo rapid motion, which averages nearly all the dipolar and chemical shift interactions. In addition, several minor resonances due to carbon atoms in 1,2-units (***v***) and trans-1,4-units (***t***) are observed in the spectra. The signals detected in PB spectrum are listed in Table S1, which reports chemical shift, calculated peak area and assignment according to Wang et al. [31]. In the pristine PB, the 97% of the polymer chains are in cis-1,4 configuration, while trans-1,4 units and 1,2 units account for 2% and 1%, respectively.

Upon the addition of SH-NBBs up to 3% wt (Fig. 3a) the spectral features only slightly change compared to pristine PB, probably due to the very low amount of employed filler. Instead, the spectra of PB/10%NBB_Xh samples display additional weak signals at 32.9 and 130.0 ppm (Fig. 3b, c). On the basis of previous studies performed by Zinan et al. on low weight model polymers, the occurrence of these signals has been associated to the transformation from cis to trans of the 1,4-units of PB chains, which induces a downfield shift (5.3–5.4 ppm) of the aliphatic peak [32]. The calculated trans-1,4 configuration accounts for 6.1 and 8.1% for PB/10% NBB_80h and PB/10%NBB_30h, respectively.

These results indicate a structural rearrangement of PB chains depending on SH-NBBs loading. In order to provide more explicit evidences on the influence of SH-NBB on the molecular structure of the polymer matrix, the same characterization has been carried out on a composite prepared *ad-hoc,* loaded with 30 wt% of SH-NBBs_80h (PB/30%NBB_80h, Fig. S3b). A remarkable increase in intensity of the signals associated to the trans-1,4 configuration of PB chains has been detected, with a calculated amount of trans-1,4 units of about 55%. Moreover, in the —CH_2— region the spectrum shows weak broad peaks at 23 and 11 ppm, attributed to the β and α methylene resonances of the mercaptopropyl chain (Si—$\underline{C}H_2$—$\underline{C}H_2$—CH_2—SH) in SH-NBBs, and a broad band at the base of the PB's methylene signals (in the range 40–20 ppm) that hinder the γ methylene resonance of the mercaptopropyl chain (Si—CH_2—CH_2—$\underline{C}H_2$—SH).

These outcomes, besides assessing the effective incorporation and the structural integrity of the silsesquioxanes units, clearly highlight a rearrangement of the PB chains induced by SH-NBBs, which probably occur also for the lowest loaded samples (e.g. for PB/3%NBB_30h and PB/3%NBB_80h).

Although no clear indications on the chemical nature of filler-polymer interactions can be inferred from the ^{13}C NMR

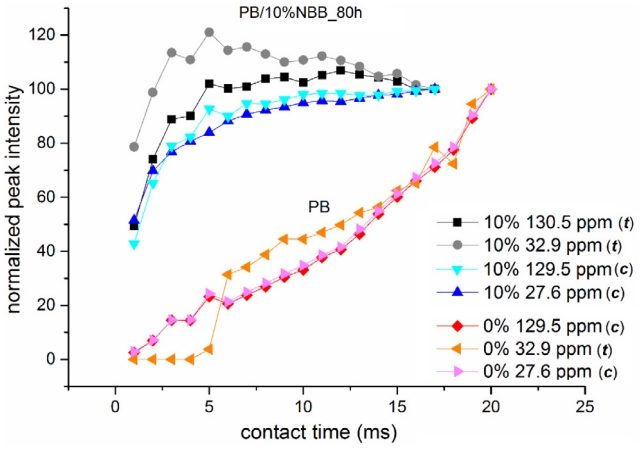

Fig. 4. ^{13}C VCT NMR curves for pure PB (bottom) and PB/10%NBB_80h (top).

investigation, the cis-to-trans conversion appears to be activated during the thermal curing of the composites as a function of the SH-NBBs loading [33,34].

In order to highlight the effect of SH-NBBs addition on chain dynamics, according to the observed increase of cross-linking density evaluated by swelling experiments (Fig. 2), variable contact time (VCT) experiments were run (Fig. 5). As a matter of facts, the peaks intensity in ^{13}C CPMAS spectra depends on the rate of cross-polarization from ^{1}H to ^{13}C nuclei. As can be clearly observed in Fig. 4 (bottom), the fast molecular motion of polymer chains in pure PB interferes with the ^{1}H-^{13}C magnetization transfer that becomes a very slow process, resulting in the increase of signal intensity at very long contact times for both cis-1,4 and trans-1,4 configurations [35].

Upon incorporation of SH-NBBs units in PB (e.g. in PB/10% NBB_80h, Fig. 4 top), the slope of the magnetization curves for the peaks related to cis-1,4 chains (27.6 and 129.5 ppm) decreases with increasing contact time, indicating a reduced mobility of the polymer. Moreover, this effect is remarkable for the peaks at 32.9 ppm and 130.5 ppm related to the trans-1,4 configuration, proving that these polymer chains are closer to the filler.

Finally, the behavior of PB/10%NBB_80h sample was also compared to that of SH-NBBs units. To this aim, the VCT curves for SH-NBBs were calculated by analyzing the α and β methylene peaks of the propyl chain (Fig. S4) that are clearly visible only in the PB/30%NBB_80h spectrum (Fig. S3b), since pure SH-NBBs are liquid. The fast decay refers to rigid objects, as expected for small highly condensed SSQs. From the comparison, it turned out that the magnetization intensity curves of PB/10%NBB_80h show a trend that is much closer to the one of SH-NBB with respect to the PB one, reasonably averaging both behaviors. This intermediate behavior presented by PB/10%NBB_80h clearly suggest that the SH-NBBs probably act as cross-linking points in the nanocomposite network, thus reducing the PB chain mobility.

In conclusion, the NMR study highlights a structural change that PB chains undergo upon SH-NBBs introduction, pointing out the probable formation of chemical interactions between polymer and active fillers by means of cross-linking reactions. Further, though the difference in the cis-to-trans conversion determined between PB/10%NBB_30h and PB/10%NBB_80h samples appears small, it can be considered a proof of an influence of the different filler architecture on the final properties of the nanocomposites.

The effect of SH-NBBs incorporation in PB on the thermal properties of the resulting nanocomposites has been investigated by TGA and DSC. Fig. 5a shows the thermogravimetric weight loss curves obtained for pure PB and for PB/Y%NBB_80h nanocomposites. All the samples display an initial weight loss beginning at nearly 350 °C and continuing until 400 °C. From 400 °C to 500 °C, a second and more evident weight loss occurs, which is less remarkable as the loading of SH-NBBs in the composites increases and clearly decreases for the composite enclosing 10 wt% of filler. This indicates an increased thermal stability of the polymer matrix after the incorporation of the SH-NBBs. Similar results were obtained for PB/%NBB_30h nanocomposites.

Fig. 5b reports the TGA curves of PB nanocomposites loaded with 3 and 10 wt% of SH-NBBs synthetized with different reaction times (30 h and 80 h). Although the thermal profiles of PB/3% NBB_30h and PB/3%NBB_80h samples appear very similar, the final weight loss is slightly different as a function of filler architecture, as demonstrated by the lack of superimposability of the curves in the range 480–600 °C. In the case of 10% loading, the experimental

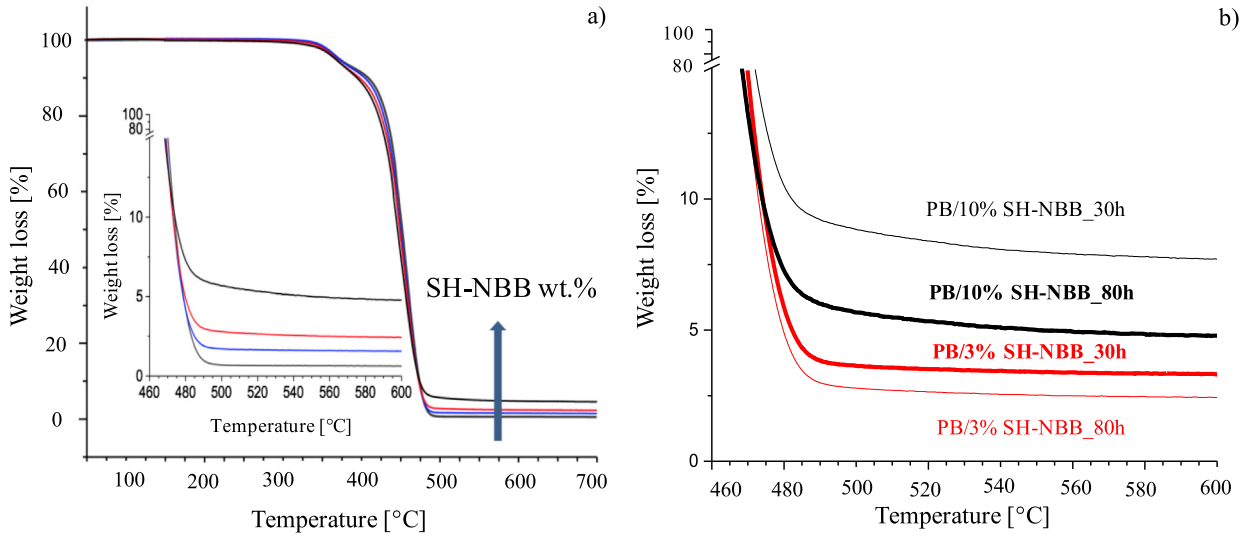

Fig. 5. TGA curves of (a) pure PB (light black line), PB/1%NBB_80h (blue line) and PB/3%NBB_80h (red line) and PB/10%NBB_80h (black line) and (b) effect of the SH-NBBs structure on the thermal properties on the nanocomposites. (For interpretation of the references to colour in this figure legend, the reader is referred to the web version of this article.)

results suggest a more effective role of SH-NBBs_30h in the polymer thermal stabilization respect to SH-NBBs_80h.

An example of typical DSC thermogram of heating/cooling DSC runs of the investigated materials is reported in Fig. S5 (PB/10%NBB_30h sample). By analyzing the plots, the following parameters can be measured. On the first heating cycle from −120 °C up to 100 °C it is possible to estimate: (i) T_{gI} corresponding to the inflection point; (ii) an exothermal peak of integral area ΔH_{cI} and peak temperature T_{cI} related to the crystallization of the PB matrix; (iii) a endothermal peak of integral area ΔH_{mI} and peak temperature T_{mI} related to the melting of the crystalline phase of the PB matrix. On the cooling step from 100 °C up to −120 °C it is possible to estimate an exothermal peak of integral area ΔH_{cc} and peak temperature T_{cc} related to the crystallization of the PB matrix. Finally, on the second heating cycle from −120 °C up to 100 °C it is possible to estimate: (i) T_{gII} corresponding to the inflection point; (ii) an exothermal peak of integral area ΔH_{cII} and peak temperature T_{cII} related to the crystallization of the PB matrix; (iii) a endothermal peak of integral area ΔH_{mII} and peak temperature T_{mII} related to the melting of the crystalline phase of the PB matrix.

The above-mentioned parameters are summarized in the following tables (Tables 1a–c) for all the investigated samples.

The results indicate that the presence of the nanofiller does not affect the glass transition temperature of the amorphous regions of the PB matrix in an appreciable way. On the other hand, remarkable effects of the nanofiller addition on the capability of the matrix to crystallize can be observed. After the previous thermal history of the samples is cancelled, i.e. at the end of first heating run (Table 1a) and during the subsequent cooling stage, it can be observed that both the crystallization temperature and crystallinity content strongly depend on the nanofiller loading (Table 1b). In particular, it can be noticed that the presence of the SH-NBBs reduces both the crystallinity content and the crystallization temperature, thus clearly indicating their ability to decrease the mobility of the macromolecules in the molten state or to increase the crosslinking degree. The effect is also corroborated by the trend of the melting enthalpies measured in the second heating stage (Table 1c). These outcomes are in agreement with both swelling and NMR characterizations, supporting a structural change of PB chains and the presence of chemical interactions between polymer and SH-NBBs upon their introduction in the polymer matrix.

DMTA analysis of PB/Y%NBBs nanocomposites were performed in order to study the effect of the filler loading and molecular architecture (cage/ladder ratio) on the mechanical properties of the nanocomposites. The obtained trends of the storage modulus E' vs temperature are summarized in Fig. 6.

Two distinct behaviors can be observed at temperatures respectively above and below the crystallization temperature. At temperatures below the crystallization temperature it can be observed that low loadings (e.g. 1 and 3 wt%) of SH-NBB units in PB/Y% NBB_80h composites induce a reinforcement of the polymer matrix, while an increase of the filler amount up to 10 wt% leads to a drop of the modulus (Fig. 6, left). A similar trend has been obtained for PB/Y%NBB_30h samples. This behavior can be attributed to the lower crystallinity that the matrix can develop in the presence of a high amount of filler.

On the contrary, in the temperature range above the melting temperature of the polymer matrix the storage modulus is increasing proportionally to the filler content, thus confirming its crosslinking effect on the polymer network.

Remarkably, by comparing the behavior of PB/3%NBB and PB/10%NBB composites enclosing SH-NBB-30h and SH-NBB-80h units (Fig. 6, right), an effect of the molecular architecture on the final properties of the composites can be also envisaged. In detail, over the entire explored temperature range, the sample PB/3% NBB_80h (higher fraction of cages in the SH-NBBs structure, red bold line), shows an higher modulus than PB/3%NBB_30h sample (higher fraction of ladder-like units in the SH-NBBs structure, black bold line), while an opposite trend is observed for PB/10%NBB_30h nanocomposites.

These results support the idea that the dispersion in PB of low loadings of SH-NBBs_80h, which contain a larger fraction of cages with high number of functionalities concentrated on the same small unit, may provide more effective interactions at the polymer-NBBs interface, resulting in enhanced performances compared to SH-NBB_30h with dominant ladder-like structure. These conclusions are well supported by the observed higher crosslinking-degree (Fig. 2), improved thermal stability (Fig. 5) and slightly reduced crystallization temperature (DSC cooling scan, Table 1b) of PB/3%NBB_80h compared to the analogous sample prepared with 3% SH-NBB_30h.

According to the NMR study, the extent of interactions between PB chains and SH-NBBs is clearly dependent on NBBs loading as assessed by the cis-to-trans conversion. However, at 10 wt% filler loading, the experimental results suggest that both structure and performances of the composites are affected by the filler aggregation, which, in turn, appears to be connected to the SH-NBBs architecture. In fact, the DMTA analysis points out that in the entire explored temperature range the storage modulus of PB/10% NBB_80h is lower than that of PB/10%NBB_30h nanocomposites, in accordance to the decrease in cross-linking degree (Fig. 2) and thermal stability (Fig. 5). Moreover, the cis-to-trans conversion

Table 1a
DSC parameters measured during the first heating scan.

Sample	First heating				
	T_{gI} (°C)	ΔH_{cI} (J/g)	T_{cI} (°C)	ΔH_{mI} (J/g)	T_{mI} (°C)
PB	−113.3	16.1	−72.5	36.5	−11.9
PB/1%NBB 30h	−112.9	1.4	−81.2	37.7	−11.7
PB/1%NBB 80h	−111.3	1.2	−76.2	37.4	−12.3
PB/3%NBB 30h	−112.0	1.4	−80.1	35.4	−13.1
PB/3%NBB 80h	−111.3	1.4	−76.9	34.9	−13.4
PB/10%NBB 30h	−112.6	24.8	−68.5	25.1	−20.4
PB/10%NBB 80h	−112.2	25.3	−70.1	25.5	−19.2

Table 1b
DSC parameters measured during the cooling scan.

Sample	Cooling	
	ΔH_{cc} (J/g)	T_{cc} (°C)
PB	44.7	−47.8
PB/1%NBB_30h	43.8	−45.6
PB/1%NBB_80h	44.1	−43.4
PB/3%NBB_30h	39.3	−46.5
PB/3%NBB_80h	41.9	−50.4
PB/10%NBB_30h	23.3	−60.6
PB/10%NBB_80h	25.2	−67.2

Table 1c
DSC parameters measured during the second heating scan.

Sample	Second heating				
	T_{gII} (°C)	ΔH_{cI} (J/g)	T_{cI} (°C)	ΔH_{mI} (J/g)	T_{mI} (°C)
PB	−110.7	0.8	−78.9	45.8	−11.9
PB/1%NBB_30h	−112.4	1.4	−70.2	45.8	−12.0
PB/1%NBB_80h	−111.5	1.6	−69.9	46.6	−12.6
PB/3%NBB_30h	−111.0	1.7	−68.1	42.1	−13.4
PB/3%NBB_80h	−111.5	1.6	−70.3	42.6	−13.6
PB/10%NBB_30h	−111.0	1.4	−69.4	25.3	−20.6
PB/10%NBB_80h	−110.2	0.6	−69.7	26.3	−19.7

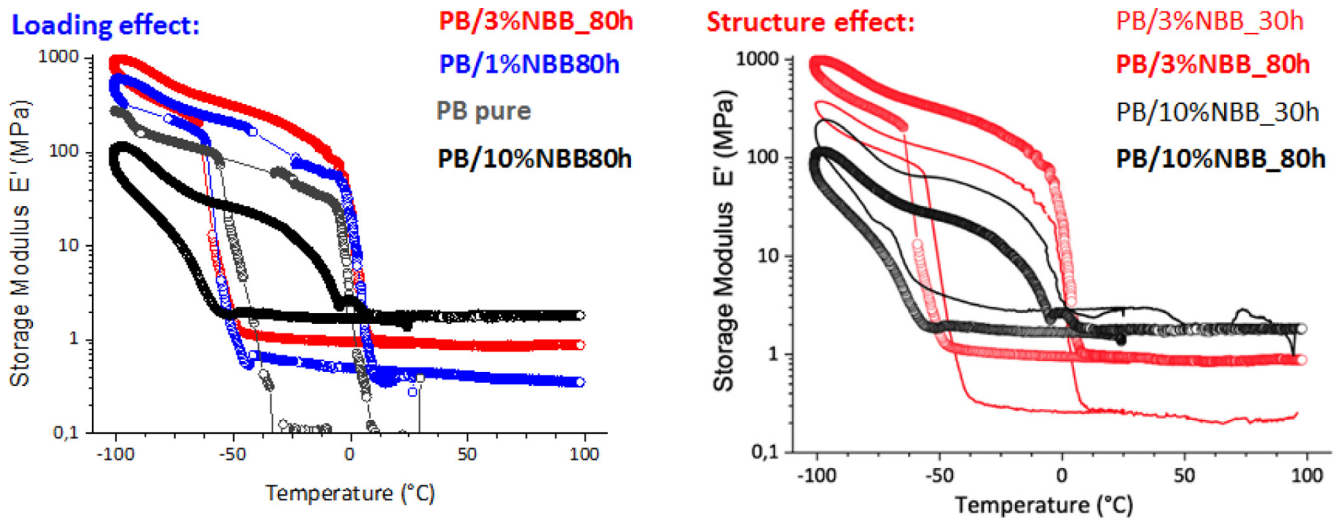

Fig. 6. (left) Trend of the storage modulus of PB/Y%NBB_80h nanocomposites as a function of the filler loading; (right) Comparison among PB/3%NBB and PB/10%NBB composites enclosing SH-NBB units obtained after a reaction time of 30 h and 80 h.

appears slightly lower in PB/10%NBB_80h than in PB/10%NBB_30h (Fig. 3). These evidences seem to indicate that the filler-filler interactions in SH-NBBs rich in cage-like structures are not only different from those occurring in filler with dominant ladder-like species, but result even detrimental to the final composites properties.

In future work, it will be informative to study in detail the aggregation phenomena in the SH-NBBs-based composites in term of size, shape, anisotropy, crystalline features of filler aggregates, even if it might not be an easy task, considering the very small dimensions of these nano-objects and the low loadings exploitable for gaining applicable materials.

4. Conclusions

In this study, hybrid nanocomposites have been prepared by a simple *solution-blending* technique using innovative fillers, SH-NBBs, with both tailorable functionalities and molecular structure (mainly cage-like or ladder-like).

FTIR, TGA, DSC, swelling and solid-state NMR analyses confirmed the successful SH-NBBs incorporation into the polymeric host and highlighted a structural change of PB chains upon filler introduction, probably connected to the occurrence of chemical interactions at the hybrid interface. Accordingly, dynamic mechanical characterization indicated that even small SH-NBBs amounts ($\leq$3 wt%) provide a remarkable enhancement of the mechanical properties, which seem to be related not only to the filler loading, but also to the peculiar molecular architecture of SH-NBBs.

In summary, beyond demonstrating that SH-NBBs are suitable nanobuilding blocks for the design of nanocomposites with improved performances, this study provides an efficient methodological protocol for shedding light on the properties at the hybrid interface between small molecular nanofillers and polymer matrix.

Acknowledgements

This work was carried out in the frame of the European COST action MP1202 "Rational design of hybrid organic-inorganic interfaces: the next step towards advanced functional materials".

M.R. thanks Corimav ("Consortium for the Research of Advanced Materials between Pirelli and Milano Bicocca University) for its support within the PCAM European Doctoral Programme.

A.P. thanks Miss Claudia Gavazza for her technical support in DSC and DMTA measurements.

M.D and M.R. gratefully acknowledge Dr. Veronica Masneri for her support in the nanocomposites preparation.

Appendix A. Supplementary material

Supplementary data associated with this article can be found, in the online version, at https://doi.org/10.1016/j.jcis.2017.10.094.

References

[1] H. Zhou, Q. Yea, J. Xu, Polyhedral oligomeric silsesquioxane-based hybrid materials and their applications, Mater. Chem. Front. 1 (2017) 212–230.
[2] E. Ayandele, B. Sarkar, P. Alexandridis, Polyhedral oligomeric silsesquioxane (POSS)-containing polymer nanocomposites, Nanomaterials 2 (2012) 445–475.
[3] K.N. Raftopoulos, K. Pielichowski, Segmental dynamics in hybrid polymer/POSS nanomaterials, Prog. Polym. Sci. 52 (2016) 136–187.
[4] S.W. Kuo, Building blocks precisely from polyhedral oligomeric silsesquioxane nanoparticles, ACS Central Sci. 2 (2016) 62–64.
[5] S.W. Kuo, F.C. Chang, POSS related polymer nanocomposites, Prog. Polym. Sci. 36 (2011) 1649–1696.
[6] A. Fina, O. Monticelli, G. Camino, POSS-based hybrids by melt/reactive blending, J. Mater. Chem. 20 (2010) 9297–9305.
[7] K. Tanaka, Y. Chujo, Advanced functional materials based on polyhedral oligomeric silsesquioxane (POSS), J. Mater. Chem. 22 (2012) 1733–1750.
[8] M. D'Arienzo, M. Redaelli, E. Callone, L. Conzatti, B. Di Credico, S. Dirè, L. Giannini, S. Polizzi, I. Schizzi, R. Scotti, L. Tadiello, F. Morazzoni, Hybrid SiO_2@POSS nanofiller: a promising reinforcing system for rubber nanocomposites, Mater. Chem. Front. 1 (2017) 212–230.
[9] S. Dirè, E. Borovin, F. Ribot, "Architecture of Silsesquioxanes", in: Handbook of Sol-Gel Science and Technology second ed., Lisa Klein, Mario Aparicio, Andrei Jitianu (Eds.), Springer (2016), https://doi.org/10.1007/978-3-319-19454-7_119-.
[10] S. Choi, A.S. Lee, S.S. Hwang, K. Baek, Structural control of fully condensed polysilsesquioxanes: ladderlike vs cage structured polyphenylsilsesquioxanes, Macromolecules 48 (2015) 6063–6070.
[11] N. Hao, M. Böhning, A. Schönhals, Nanocomposites of polyhedral oligomeric phenethylsilsesquioxanes and Poly(bisphenol A carbonate) as investigated by dielectric spectroscopy, Macromolecules 40 (2007) 9672–9679.
[12] A. Bele, M. Dascalu, C. Tugui, I. Mihailla, R. Carmen, L. Sacarescu, M. Cazacu, Dielectric silicone elastomers filled with in situ generated polar silsesquioxanes: preparation, characterization and evaluation of electromechanical performance, Mater. Design 106 (2016) 454–462.
[13] K.N. Raftopoulos, S. Koutsoumpis, M. Jancia, J.P. Lewicki, K. Kyriakos, H.E. Mason, S.J. Harley, E. Hebda, C.M. Papadakis, K. Pielichowski, P. Pissis, Reduced phase separation and slowing of dynamics in polyurethanes with three-dimensional POSS-based cross-linking moieties, Macromolecules 48 (2015) 1429–1441.
[14] L. Matějka, I.A. Kroutilová, J.D. Lichtenhan, T.S. Haddad, Structure ordering and reinforcement in POSS containing hybrids, Eur. Polym. J. 52 (2014) 117–126.

[15] A.S. Lee, S.S. Choi, H.S. Lee, K.Y. Baek, S.S. Hwang, A new, higher yielding synthetic route towards dodecaphenyl cage silsesquioxanes: synthesis and mechanistic insights, Dalton Trans. 41 (2012) 10585–10588.
[16] A.S. Lee, S.S. Choi, H.S. Lee, K.Y. Baek, S.S. Hwang, High photo- and electroluminescence efficiencies of ladder-like structured polysilsesquioxane with carbazole groups, J. Mater. Chem 20 (2010) 9852–9854.
[17] A.S. Lee, S.S. Choi, H.S. Lee, K.Y. Baek, S.S. Hwang, Synthesis and characterization of UV-curable ladder-like polysilsesquioxane, J. Polym. Sci. Part A: Polym. Chem. 49 (2011) 5012–5018.
[18] A.S.S. Lee, J.H. Lee, J. Lee, S.M. Hwang, C. Min Koo, Novel polysilsesquioxane hybrid polymer electrolytes for lithium ion batteries, J. Mater. Chem. A 2 (2014) 1277–1283.
[19] K.Y. Cho, A.S. Lee, H. Jeon, S. Park, M. Jang, H. Yoon, S. Hong, K. Baek, S.S. Hwang, Tuning the interface between poly(vinylidene fluoride)/UV-curable polysilsesquioxane hybrid composites: compatibility, thermal, mechanical, electrical, and surface properties, Polymer 77 (2015) 167–176.
[20] L. Liu, Y. Yuan, Y. Huang, H. Yu, J. Yang, A new mechanism for the low dielectric property of POSS nanocomposites: the key role of interfacial effect, Phys. Chem. Chem. Phys 19 (2017) 14503–14511.
[21] L. Wahba, M. D'Arienzo, R. Donetti, T. Hanel, R. Scotti, L. Tadiello, F. Morazzoni, In situ sol–gel obtained silica – rubber nanocomposites: influence of the filler precursors on the improvement of the mechanical properties, RSC Adv. 3 (2013) 5832–5844.
[22] R. Scotti, L. Wahba, M. Crippa, M. D'Arienzo, R. Donetti, N. Santo, F. Morazzoni, A novel non-aqueous sol-gel route for the in situ synthesis of high loaded silica-rubber nanocomposites, Soft Matter 8 (2012) 2131–2143.
[23] R. Scotti, L. Conzatti, M. D'Arienzo, B. Di Credico, L. Giannini, T. Hanel, P. Stagnaro, A. Susanna, L. Tadiello, F. Morazzoni, Shape controlled spherical (0D) and rod-like (1D) silica nanoparticles in silica/styrene butadiene rubber nanocomposites: role of the particle morphology on the filler reinforcing effect, Polymer 55 (2014) 1497–1506.
[24] L. Tadiello, M. D'Arienzo, B. Di Credico, T. Hanel, L. Matejka, M. Mauri, F. Morazzoni, R. Simonutti, M. Spirkova, R. Scotti, The filler-rubber interface in styrene butadiene nanocomposites with anisotropic silica particles: morphology and dynamic properties, Soft Matter 11 (2015) 4022–4033.
[25] O. Bianchi, L.G. Barbosa, G. Machado, L.B. Canto, R.S. Mauler, R.V.B. Oliveira, Reactive melt blending of PS-POSS hybrid nanocomposites, J. Appl. Polym. Sci. 128 (2013) 811–827.
[26] E. Borovin, E. Callone, B. Papendorf, G. Guella, S. Diré, Influence of sol-gel conditions on the growth of thiol-functionalized silsesquioxanes prepared by in situ water production, J. Nanosci. Nanotechnol. 16 (2016) 3030–3038.
[27] E. Borovin, E. Callone, F. Ribot, S. Diré, Mechanism and kinetics of oligosilsesquioxane growth in the in situ water production sol-gel route: dependence on water availability, Eur. J. Inorg. Chem. 2166–2174 (2016).
[28] B.W. Ellis, G.N. Welding, Estimation, from swelling, of the structural contribution of chemical reactions to the vulcanization of natural rubber. Part II. estimation of equilibrium degree of swelling, Rubber Chem. Technol. 37 (1964) 571–575.
[29] P.J. Flory, J. Rehner, Statistical mechanics of cross- linked polymer networks II, J. Chem. Phys. 11 (1943) 521–526.
[30] R.A. Orwoll, P.A. Arnold, Physical Properties of Polymers Handbook J.E. Mark (Ed.), AIP Press, New York, 1996.
[31] H.-T. Wang, T.W. Bethea, H.J. Hardwood, Narrow molecular weight resins by a free-radical polymerization process, Macromolecules 26 (1993) 715–720.
[32] N. Makhiyanov, M.M. Minnegaliev, R.M. Aminova, ^{13}C NMR chemical shifts and local structure of cis-1,4-polybutadiene: calculation and experiment, Polym. Sci. Series A 58 (2016) 121–129.
[33] E.C. Gregg Jr, R.P. Lattimer, Polybutadiene vulcanization. chemical structures from sulfur-donor vulcanization of an accurate model, Rubber Chem. Technol. 57 (1984) 1056–1097.
[34] S.S. Choi, Y. Kim, H. Kwon, Microstructural analysis and cis – trans isomerization of BR and SBR vulcanizates reinforced with silica and carbon black using NMR and IR, RSC Adv. 4 (2014) 31113–31119.
[35] M.R.G. Coelho, R.A.S. San Gil, M.I.B. Tavaresbv, Carbon-13 high-resolution solid state NMR study of polybutadiene, Polym. Testing 15 (1996) 485–490.